# Spreading of a local excitation in a quantum hierarchical model

Luca Capizzi,[1,2,*] Guido Giachetti,[1,2,†] Alessandro Santini ®,[1,‡] and Mario Collura[1,2,§]

[1]*SISSA, via Bonomea 265, 34136 Trieste, Italy*
[2]*INFN, Sezione di Trieste, via Bonomea 265, 34136 Trieste, Italy*

We study the dynamics of the quantum Dyson hierarchical model in its paramagnetic phase. An initial state made by a local excitation of the paramagnetic ground state is considered. We provide analytical predictions for its time evolution, solving the single-particle dynamics on a hierarchical network. A localization mechanism is found, and the excitation remains close to its initial position at arbitrary times. Furthermore, a universal scaling among space and time is found that is related to the algebraic decay of the interactions as $r^{-1-\sigma}$. We compare our predictions to numerics, employing tensor network techniques, for large magnetic fields, discussing the robustness of the mechanism in the full many-body dynamics.

## I. INTRODUCTION

Long-range-interacting systems, characterized by slow-decaying power-law potentials, are known to exhibit a plethora of peculiar behaviors [1], including dynamical phase transitions [2,3], long-lived metastable states [1,4,5], time crystalline phases [2,6–9], peculiar critical properties in low dimensions [10,11], exotic defect scaling [12,13], and slow entanglement propagation [14–18]. This phenomenology stimulated impressive theoretical activity aimed at understanding the equilibrium and nonequilibrium behavior of such systems [19–21]. Examples of long-range physics can be observed across several fields of physics from astrophysics [1,22,23] to plasma physics [24] and fluid dynamics [25]; they also have been engineered in experimental setups based on atomic, molecular and optical systems (AMO) [21], trapped ions [19,26], Rydberg gases [27], and optical cavities [20,28].

In this context, the classical hierarchical model was originally introduced by Dyson in his seminal paper [29] as a tool for understanding the critical properties of one-dimensional long-range spin systems. Here the usual translational-invariant adjacency matrix of the couplings is replaced by those of a hierarchical network, allowing us to explicitly carry out the renormalization group procedure [30]. A quantum counterpart of the hierarchical Ising model, in which the classic spin variables are replaced with noncommuting spin operators, has been proposed in [31]. The strong disorder renormalization group (SDRG) [32] can be used to understand the ground-state properties of the hierarchical quantum Ising model in a transverse magnetic field [33] and its entanglement content [34].

We also mention that a relation between the hierarchical models and a field theoretical formulation in fractal spaces has been proposed, and it is still a current topic of research in the context of high-energy physics. In particular, we refer to the characterization of adelic string amplitudes [35] together with a *p*-adic formulation of the anti-de Sitter/conformal field theory AdS/CFT correspondence [36–38], where the complex field $\mathbb{C}$ is replaced by the *p*-adic field $\mathbb{Q}_p$.

In this work, we focus on the dynamics of the hierarchical quantum Ising model in the paramagnetic regime. We consider an initial state made by a localized excitation, and we study its time evolution. We find that the lack of translational invariance, replaced here by a hierarchical tree structure, results in the localization of the excitation around its initial position. In addition, thanks to the presence of a self-similar structure of the Hamiltonian, a scaling relation between space and time ($t \sim x^z$) is found which differs from the one at criticality [31].

This paper is organized as follows: in Sec. II we introduce the model as a quantum chain with tree-structured long-range interactions. In Sec. III we focus on the dynamics of the localized excitation in the paramagnetic phase, which turns out to be equivalent to a Schrödinger equation in the presence of a hierarchical long-range hopping. The evolution of the single-particle wave function is thus constructed explicitly, and its properties of localization are discussed rigorously. In Sec. IV we compare our analytical predictions, which are exact in a proper scaling limit, with the evolution of a finite chain, obtained via numerical techniques, and we find very good agreement. Finally, we draw our conclusions in Sec. V and report some additional details in the Appendixes.

## II. MODEL

We consider a one-dimensional spin-1/2 lattice of length $L = 2^N$. We can arrange the spins in $N + 1$ possible binary partitions $\pi_p$ whose elements are composed of collections of consecutive and adjacent $2^p$ spins. We may define by $(j, \ldots, j')$ an element of a certain partition $\pi_p$ which contains all the spins from position $j$ to $j'$. In particular, at the lowest level $p = 0$, the partition $\pi_0$ contains $L$ elements $(1), (2), \ldots, (L)$. Then, $\pi_1$ contains $L/2$

*lcapizzi@sissa.it
†ggiachet@sissa.it
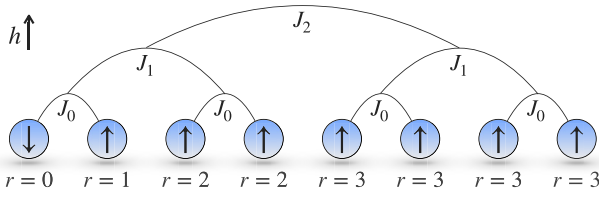‡asantini@sissa.it
§mcollura@sissa.it

FIG. 1. Schematic representation of the hierarchical Dyson model for $N = 3$, where the branches of the binary tree highlight the structure of the interactions. We show the hierarchical distances from the first site $r \equiv r(1, j)$.

blocks $(1, 2), (3, 4), \ldots, (L − 1, L)$, $\pi_2$ contains $L/4$ blocks $(1, 2, 3, 4), (5, 6, 7, 8), \ldots, (L − 3, L − 2, L − 1, L)$, and so on, up to the final partition $\pi_N$, whose only element is the whole chain $(1, 2, 3, \ldots, L)$.

We can distinguish an element of a partition by a pair $(p, q)$, where $p$ identifies the partitioning level while $q$, $q = 1, \ldots, 2^{N−p}$, runs over the elements of $\pi_p$. For each element $(p, q)$ we identify the collective spin

$$\mathbf{S}_{(p,q)} \equiv \sum_j \boldsymbol{\sigma}_j, \quad (q − 1)2^p + 1 \leqslant j \leqslant q2^p, \quad (1)$$

where $\boldsymbol{\sigma}_j = (\sigma_j^x, \sigma_j^y, \sigma_j^z)$ is the vector of the Pauli matrices at position $j \in \{1, \ldots, L\}$.

We can now define the Hamiltonian of the quantum hierarchical Dyson model as

$$H = −\sum_{p=0}^{N−1} \sum_{q=1}^{2^{N−p−1}} J_p S_{(p,2q−1)}^x S_{(p,2q)}^x − h S_{(N,1)}^z, \quad (2)$$

where $J_p = J/2^{(1+\sigma)p}$ represents the interaction term at level $p$. A sketch of the model is schematically represented in Fig. 1. Let us notice that the term proportional to $h$ represents the coupling with a uniform transverse magnetic field since $S_{(N,1)}^z = \sum_{j=1}^{2^N} \sigma_j^z$, while the longitudinal interaction along the $x$ axis among distinct spins is introduced so that it displays a hierarchical structure. For the sake of convenience, we define a hierarchical distance $r(i, j)$ as the minimum level $p$ for which sites $i$ and $j$ belong to the same element of the partition $\pi_p$ [e.g., $r(1, 1) = 0, r(1, 2) = 1, r(1, 3) = r(1, 4) = 2$, and so on]. In this way, we can rewrite the Hamiltonian (2) as

$$H = −\sum_{i<j} J_{r(i,j)−1} \sigma_i^x \sigma_j^x − h \sum_i \sigma_i^z, \quad (3)$$

explicitly showing how the interaction among different spins depends on the distance $r(i, j)$, instead of the Euclidean one $|i − j|$. To relate these two quantities, we may roughly estimate $|i − j| \approx 2^{r(i,j)}$, which means that the coupling strength of the model scales as

$$J_{r(i,j)−1} = \frac{J}{2^{(1+\sigma)(r(i,j)−1)}} \approx \frac{J}{|i − j|^{1+\sigma}}. \quad (4)$$

From now on we will restrict the analysis of the model to $\sigma > 0$.

## III. LOCALIZATION

In this section, we investigate the dynamics of the model in the paramagnetic phase, in particular in the limit of a large magnetic field $h \gg J$. Due to the separation of scales, states with distinct values of the total magnetization along $z$ are effectively decoupled, and thus, we may refer to $S_{(N,1)}^z$ as a quasiconserved charge. Above the fully polarized paramagnetic state, namely, $|\uparrow \ldots \uparrow\rangle$, we can create excitations via local spin flips. We interpret these excitations as states with particles localized at some points along the chain. In this regime, the dynamics is equivalent to the one induced by the following hard-core boson (effective) Hamiltonian:

$$H = −\sum_{i<j} J_{r(i,j)−1} (b_i^\dagger b_j + b_j^\dagger b_i), \quad (5)$$

where $b_i^\dagger$ and $b_i$ are the creation and annihilation operators of hardcore bosons, satisfying $[b_i, b_j] = [b_i^\dagger, b_j^\dagger] = 0$, $[b_i, b_j^\dagger] = \delta_{i,j}$, with the additional constraint $b_j^2 = (b_j^\dagger)^2 = 0$. Notice that, even if this description is exact only for $h/J \to +\infty$, the qualitative picture is kept unchanged as long as $h/J$ is large enough to ensure that the system is sufficiently deep in the paramagnetic phase (see [39] for further details).

We are interested in the dynamics induced by a strongly paramagnetic Hamiltonian after a local excitation (spin flip) has been created on top of the fully polarized state. Namely, we prepare the system in the initial configuration $|\psi(0)\rangle = |\downarrow\uparrow\uparrow \ldots \uparrow\rangle$, and then we let it evolve in time and thus analyze the spreading of a single particle initially localized in the first lattice site. Let us mention that the position of the initial spin flip is unimportant since the chain is homogeneous: indeed, despite the lack of translational symmetry, the Hamiltonian is invariant under permutations of sites that keep the hierarchical distance $r(i, j)$ fixed.

The protocol under consideration is simple enough to be exactly solvable, and the thermodynamic limit can be analyzed. We expect that the resulting picture is able to capture the salient features of the whole paramagnetic phase, and it should be predictive if the particles are diluted enough. Moreover, some crucial properties, which depend mostly on the tree structure of the Hamiltonian, are highlighted, and possibly, they are shared by any hierarchical model, irrespective of the microscopic details. In this regime, the dynamics remains in the single-particle sector, and the projected Hamiltonian (5) can be exactly diagonalized.

In the following, to simplify the notation, we introduce $r \equiv r(1, j)$ as the hierarchical distance between the $j$th state and the first site. Moreover, we describe a generic one-particle state $|\Psi(t)\rangle = \sum_{x=1}^L \psi(x, t) |x\rangle$ via its associated wave function $\psi(x, t) = \langle x \rangle \Psi(t)$, where $|x\rangle$ represents a state with a single particle (spin flip) localized at position $x$ on the chain. As a consequence, the initial state $|\Psi(0)\rangle$ is simply characterized by the $\delta$-peaked wave function $\psi(x, 0) = \delta_{x,1}$. We can decompose further the initial wave function in terms of the eigenfunctions of the single-particle Hamiltonian (see Appendix A), obtaining

$$\psi(x, 0) = \frac{1}{L} \chi_{[1,L]}(x) \quad (6)$$

$$+ \frac{1}{L} \sum_{k=1}^{N} 2^{k-1} [\chi_{[1,L/2^k]}(x) - \chi_{[1+L/2^k, L/2^{k-1}]}(x)], \tag{7}$$

where $\chi_{[a,b]}(x)$ is the characteristic function of the interval $[a, b]$ and is defined as

$$\chi_{[a,b]}(x) = \begin{cases} 1 & x \in [a, b], \\ 0 & \text{otherwise}. \end{cases} \tag{8}$$

Through the previous decomposition, we can easily express the time-evolved state as

$$\psi(x, t) = \frac{1}{L} \chi_{[1,L]}(x) e^{-i\epsilon_0 t} + \frac{1}{L} \sum_{k=1}^{N} e^{-i\epsilon_k t} 2^{k-1}$$

$$\times [\chi_{[1,L/2^k]}(x) - \chi_{[1+L/2^k, L/2^{k-1}]}(x)], \tag{9}$$

with $\epsilon_k$ being the single-particle energies,

$$\epsilon_k = -\frac{J}{1 - 2^{-\sigma}} \left(1 - \frac{2^{k\sigma}}{L^\sigma}\right) + J \frac{2^{k\sigma}}{L^\sigma} (1 - \delta_{k,0}). \tag{10}$$

Here $k = 0, \dots, N$ labels, in ascending order, only the distinct eigenvalues of the coupling matrix, whose dimension is $2^N$. Apart from the first two nondegenerate eigenvalues, it can be seen (see Appendix A) that all the others have degeneracy $2^{k-1}$, such that $1 + \sum_{k=1}^{N} 2^{k-1} = 2^N$.

Since the value of the wave function at position $x$ depends only on the hierarchical distance $r = \lfloor \log_2(x) \rfloor$, it is convenient to write it explicitly as a function of only $r$ and $t$, denoting it as $\psi(r, t)$ (with a slight abuse of notation). For $r > 0$ its expression reads

$$\psi(r, t) = \frac{1}{L} e^{-i\epsilon_0 t} + \frac{1}{L} \sum_{k=1}^{N-r} 2^{k-1} e^{-i\epsilon_k t} - 2^{-r} e^{-i\epsilon_{N-r+1} t}, \tag{11}$$

while for $r = 0$ we have

$$\psi(0, t) = \frac{1}{L} e^{-i\epsilon_0 t} + \frac{1}{L} \sum_{k=1}^{N} 2^{k-1} e^{-i\epsilon_k t}. \tag{12}$$

### A. Scaling limit with $r$ fixed and $N \to +\infty$

So far, we have derived an expression for the evolution of the state localized at the first position [see Eqs. (11) and (12)], which is exact for any length $L = 2^N$ of the chain as long as $h/J \to +\infty$. Now, we want to understand what happens in the thermodynamic limit $N \to \infty$. It should be clear from the explicit expression of the sum in Eq. (12) that the dominant contributions come from the large values of $k$, namely, the high-energy (single-particle) modes. For this reason, it is rather natural to change the variable $k \to N - k$, so that the first terms of the sum become the relevant ones, and we can thus approximate the sum as series in the large-$N$ limit. Under this change in variable, the single-particle spectrum can be parameterized for large $N$ (up to an irrelevant additive constant) as

$$\varepsilon_k = \tilde{J}_\sigma 2^{-\sigma k} + \text{const}, \quad \tilde{J}_\sigma \equiv J \frac{2^{\sigma+1} - 1}{2^\sigma - 1}. \tag{13}$$

We remark explicitly that $\varepsilon_k = \epsilon_{N-k}$, and we use a distinct symbol to avoid confusion. We now keep $r$ fixed, send $N \to +\infty$, and analyze how $\psi(r, t)$ behaves in time as a function of $Jt$. We first consider $r = 0$, for which we have

$$\psi(0, t) = \frac{e^{-i\epsilon_0 t}}{L} + \sum_{k=0}^{N-1} 2^{-k-1} e^{-i\varepsilon_k t}. \tag{14}$$

The sum above converges exponentially fast as $N \to \infty$ to a finite value that we write as

$$\psi(0, t) \simeq \sum_{k=0}^{\infty} 2^{-k-1} e^{-it\varepsilon_k} = \sum_{k=0}^{\infty} 2^{-k-1} e^{-i\tilde{J}_\sigma t 2^{-\sigma k}}. \tag{15}$$

Similarly, for $r \geq 1$ we get

$$\psi(r, t) = \sum_{k=r}^{\infty} 2^{-k-1} e^{-it\varepsilon_k} - 2^{-r} e^{-it\varepsilon_{r-1}}$$

$$= 2^{-r} [\psi(0, 2^{-\sigma r} t) - e^{-i\tilde{J}_\sigma t 2^{-\sigma(r-1)}}]. \tag{16}$$

The above analytical expressions are one of the main findings of our work, which in turn result in the localization of the initial spin flip around its original position.

We show this in Fig. 2, where we plot, for the representative values $\sigma = 0.5, 1, 2$, the time evolution of the absolute square of the single-particle wave function in the thermodynamic limit for a few lattice positions.

We notice that the exponential convergence of the series defining $\psi(0, t)$ is a feature that does not rely on the explicit expression of the single-particle energies $\varepsilon_k$, only on the shape of the single-particle eigenfunctions. The latter are distinct from plane waves, which typically occur in translationally invariant systems, and they are a feature of hierarchical models (displaying the symmetries of a Bruhat-Tits tree). A striking consequence is that $|\psi(0, t)|^2$, which is the return probability, oscillates on a typical timescale $\sim J^{-1}$ independent of the system size: this mechanism is already a feature of a localized system.

If we keep track of the precise details of the interactions, using $\varepsilon_k$ in Eq. (13) as single-particle spectrum, the dynamics additionally shows scale invariance. More precisely, we have, for $r > 0$,

$$\psi(r, t) = 2^{-r} F(t 2^{-\sigma r}), \tag{17}$$

with $F(t) = \psi(0, t) - e^{-i\tilde{J}_\sigma 2^\sigma t}$ being a universal function which depends on only $\sigma$ and $Jt$. The scaling in Eq. (17) can be better understood if the hierarchical distance $r$ is compared to the Euclidean one. Restricting the analysis to a position $x$ on the chain which is an integer power of 2, say, $x = 2^r$, we find that the hierarchical distance between $x$ and the first site is exactly $r$. This means that we can write Eq. (17) as

$$\psi(x, t) \sim \frac{1}{x} F(t x^{-\sigma}). \tag{18}$$

The scaling above makes transparent the presence of a dynamical exponent $z \equiv \sigma$, which relates time and space as $t \sim x^z$. Finally, it is worth mentioning that the value of $z$ we observe is eventually related to the paramagnetic phase of the model (we are assuming $h \gg J$) and it differs explicitly from the dynamical exponent at the critical point (investigated in Ref. [39]).
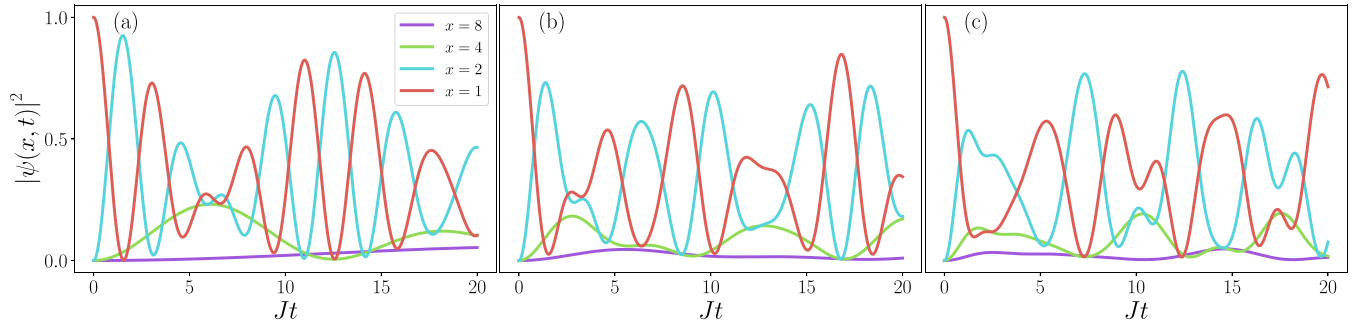
FIG. 2. Analytical prediction for the single-particle probability distribution as a function of time $t$ and site $x$, given by Eqs. (15) and (16). We show (a) $\sigma = 2$, (b) $\sigma = 1$, and (c) $\sigma = 0.5$.

### B. Time averages and upper bound

In the previous section, we did not use the specific details of the universal function $F$ in Eq. (17), except that it is limited and it oscillates in time with a typical timescale $\sim J^{-1}$. This section aims to investigate exactly some features related to the time averages and the upper bounds of the probability distribution to better quantify the localization properties of our dynamical protocol.

For any site $j$ of the lattice at hierarchical distance $r = r(1, j)$ from the first one, the probability that the particle is found at position $j$ at time $t$ is $|\psi(r, t)|^2$. A straightforward computation shows that for $r \geqslant 1$ the number of lattice sites at hierarchical distance $r$ from the first site is exactly $2^{r-1}$. This means that the probability of finding the defect in a generic site at distance $r$ is given by

$$P(r, t) \equiv \begin{cases} 2^{r-1}|\psi(r, t)|^2 & r \geqslant 1, \\ |\psi(0, t)|^2 & r = 0. \end{cases} \tag{19}$$

Let us now consider the long-time average of the probability $P(r, t)$, defined as

$$\langle P(r, t) \rangle \equiv \lim_{T \to \infty} \frac{1}{T} \int_0^T P(r, t) dt. \tag{20}$$

We will show that for any given $r$ and in particular for $r = 0$, this long-time average is finite in the thermodynamic limit $L \to \infty$. Let us first compute $\langle P(0, t) \rangle$, for which we have

$$\langle P(0, t) \rangle = \frac{1}{4} \sum_{k,k'} 2^{-k-k'} \langle e^{-i\tilde{J}_\sigma t(2^{-k\sigma} - 2^{-k'\sigma})} \rangle. \tag{21}$$

Since the single-particle energies $\varepsilon_k$ differ for different $k$, the coherence terms vanish in the long-time average, and we get $\langle e^{-i\tilde{J}_\sigma t(2^{-k\sigma} - 2^{-k'\sigma})} \rangle = \delta_{k,k'}$. This results in

$$\langle P(0, t) \rangle = \frac{1}{4} \sum_{k=0}^{\infty} 2^{-2k} = \frac{1}{3}. \tag{22}$$

A similar calculation shows

$$\langle P(r, t) \rangle = \frac{2^{1-r}}{3}, \quad r \geqslant 1. \tag{23}$$

As a consistency check, we can easily verify $\sum_{r=0}^{\infty} \langle P(r, t) \rangle = 1$. From the results in Eqs. (22) and (23), we learn that the particle can be found, on average, with probability $1/3$ in both

the first and second sites (represented by $r = 0$ and $r = 1$, respectively), which is also the average probability of finding it at hierarchical distance $r \geqslant 2$. More generally, the probability of finding the particle at hierarchical distance $r$ greater than $R$ is

$$\langle P(r > R, t) \rangle \equiv \sum_{r=R+1}^{\infty} \langle P(r, t) \rangle = \frac{2^{1-R}}{3}, \tag{24}$$

which is exactly the average probability that it is at distance $r = R$ [see (23)]. We comment explicitly that if the time $T$, appearing in the definition of the time average in Eq. (20), is kept finite, then the agreement with our predictions [Eqs. (22) and (23)] is expected to hold only up to a hierarchical distance $r$ such that $2^{r\sigma} \ll JT$. As a consequence, the more distant the position is from the first site, the slower the relaxation is (on average). This observation explains why the long-time averages do not depend explicitly on the parameter $\sigma$, which may look like a counterintuitive property at first sight.

Beyond the probability averages, we also provide some upper bounds on $P(r, t)$ valid for any $t$. Indeed, for $r > 0$ we have $|\psi(r, t)| \leqslant 2^{-r}[1 + |\psi(0, t)|] \leqslant 2^{1-r}$, where the triangular inequality has been used, together with $|\psi(0, t)| \leqslant 1$. Finally, we can show the probability of being at a hierarchical distance $r > R$ can be bounded by

$$P(r > R, t) \leqslant 2^{1-R}. \tag{25}$$

As a matter of fact, the local excitation is localized around the first sites, not only on average but also for any time $t$ no matter how large it is.

### C. Singular limit $\sigma \to 0$

The predictions provided so far refer to any finite value of $\sigma > 0$. Here we investigate the limit $\sigma \to 0$, which has to be handled carefully due to divergence at the level of the single-particle energies $\varepsilon_k$ in Eq. (13). Despite this divergence, we show that $|\psi(r, t)|^2$ has a well-defined limit for $\sigma \to 0$ and fixed $Jt$.

By expanding $\varepsilon_k$ for small $\sigma$, we get

$$\varepsilon_k = J\left(\frac{1}{\sigma \ln 2} + \frac{3}{2} - k\right) + O(\sigma), \tag{26}$$

where the diverging term for $\sigma \to 0$ enters only as an additive constant and it contributes as an irrelevant global phase on the

wave function $\psi(r,t)$. By getting rid of it, we find

$$\psi(0,t)|_{\sigma=0} = \frac{1}{2 - e^{iJt}}, \qquad (27)$$

while for $r \geqslant 1$

$$\psi(r,t)|_{\sigma=0} = 2^{1-r} e^{iJrt} \frac{1 - e^{-iJt}}{2 - e^{iJt}}. \qquad (28)$$

Similarly, the probability reads

$$P(r,t)|_{\sigma=0} = \begin{cases} \frac{1}{5 - 4\cos Jt} & r = 0, \\[2mm] 2^{-r} \frac{4 - 4\cos Jt}{5 - 4\cos Jt} & r \geqslant 1. \end{cases} \qquad (29)$$

The latter results show that in this limit the evolution of $P(r,t)$ is periodic with a period $2\pi/J$, which does not depend on $r$. This is compatible with the rough estimation of the recurrence time $\sim J^{-1} 2^{r\sigma}$ from scaling arguments.

We finally emphasize that the finite value we get relies on the fact that $J$ has been kept fixed in the thermodynamic limit $N \to \infty$ and $\sigma \to 0$. As a matter of fact, it turns out that the critical value of $h/J$, above which the model is in the paramagnetic phase, goes to infinity as $\sigma \to 0$ (see [39]). This means, in practice, that for small $\sigma$ we need huge values of the magnetic field in order to observe the single-particle regime we have described so far. We could, in principle, overcome this issue by a redefinition $J \to J\sigma$ (Kac's rescaling). However, with the latter prescription the typical relaxation time would be $\sim \sigma^{-1} J^{-1}$, thus diverging for $\sigma \to 0$. As a consequence, the system would be frozen forever in the initial state for $\sigma \to 0$. These observations indicate that, despite the finite value of $P(r,t)|_{\sigma=0}$ in Eq. (29), the limit $\sigma \to 0$ remains somehow pathological.

## IV. NUMERICAL RESULTS

In order to explore the effects of finite $h$ we used a suitable matrix product state (MPS) representation of the many-body wave function, combined with the corresponding matrix product operator (MPO) representation of the Hamiltonian [40]. The nonequilibrium dynamics has been computed via the time-dependent variational principle (TDVP) algorithm [41–43].

In particular, we considered the two-site TDVP algorithm with $dt = 0.01$; the long-range MPO is constructed through a finite-state machine [44]. Then, we compressed the MPO's bond dimension with singular-value decompositions [45]; thanks to the hierarchical structure of the interactions, the resulting bond dimension after the compression is less than 10, and thus it is greatly reduced. In our simulation we used the MPS's max bond dimension $\chi = 64$, which in the worst case produced a truncation error of order $10^{-6}$.

Thanks to the symmetries of the model and the quasi-conserved charge $S^z_{(N,1)}$, the entanglement produced during our dynamical protocol grows quite slowly, and the MPS description allows us to reach very large times. In addition, to make a connection to the full many-body dynamics at finite $h$, we notice that the expectation value of the local number of excitations can be related to the local magnetization as follows:

$$n(x,t) = \tfrac{1}{2}[1 - \langle \Psi(t)|\sigma^z(x)|\Psi(t)\rangle], \qquad (30)$$
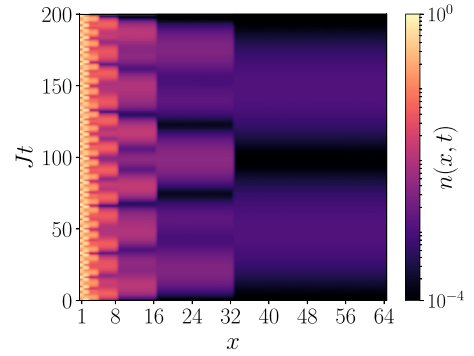


FIG. 3. TDVP simulations of the average number of particles at position $x$ and time $t$. A chain of length $L = 2^6 = 64$ has been chosen, and the parameters are $\sigma = 1$ and $h = 40J$.

while the many-body equivalent of the definition of $P(r,t)$ is

$$P(r,t) = \begin{cases} 2^{r-1} n(r,t) & r \geqslant 1, \\[2mm] n(0,t) & r = 0. \end{cases} \qquad (31)$$

As $h \gg J$, the single-particle picture is justified, and we have $n(x,t) \approx |\psi(x,t)|^2$. This is the case in Fig. 3, in which we show the evolution of $n(x,t)$ for $h = 40J$ and $\sigma = 1$. In agreement with Eq. (18), the dynamics is localized in the first few sites, and the defect is unable to spread along the tree. Moreover, since $h$ is pretty large, $S^z_{(N,1)}$ is well conserved. The sites which are farther from the initial position of the defect, along the branches of the binary tree, show exponentially slow dynamics and a suppressed wave-function modulus.

In Fig. 4 we show the evolution of the time-averaged probability $\langle P(r,t)\rangle$ as a function of $JT$ for some values of $h$ and $\sigma = 1, 2$. The dashed horizontal lines mark the theoretical predictions for strong field given in Eq. (23). In addition, in Fig. 5 we plot $\langle P(r,t)\rangle$ as a function of $r$ for some values of $h$ for large enough values of $JT$ that the average number of particles is settled to a stationary value. As expected, for decreasing values of $h$, the number of defects along the chain is no longer a conserved quantity, i.e.,

$$\sum_{x=1}^{L} \frac{1}{2}[1 - \langle \Psi(t)|\sigma^z(x)|\Psi(t)\rangle] \neq 1. \qquad (32)$$

Thus, pair production becomes important, and the full many-body state starts to leave the single spin-flip manifold. We note that for small values of $r < 3$ the prediction also holds for values of $h$ not that far from the critical value $h_c$, i.e., $h_c(\sigma = 2) \approx 0.52J$ and $h_c(\sigma = 1) \approx 1.28J$ [39]. On the other hand, at large distances and for small values of the transverse field $h$, the agreement with the single-particle approximation gets worse since the pair production becomes the relevant mechanism in generating defects.

Finally, in Fig. 6, we inspect how the universality relation in Eq. (17) gets violated by varying the magnetic field $h$ and the hierarchical distance $r$. Again, we find good agreement with the single-particle prediction for small values of $r$ (apart from small deviations due to finite-size effects) up to larger rescaled times $2^{-r\sigma} Jt$, as long as we keep $h$ sufficiently large.
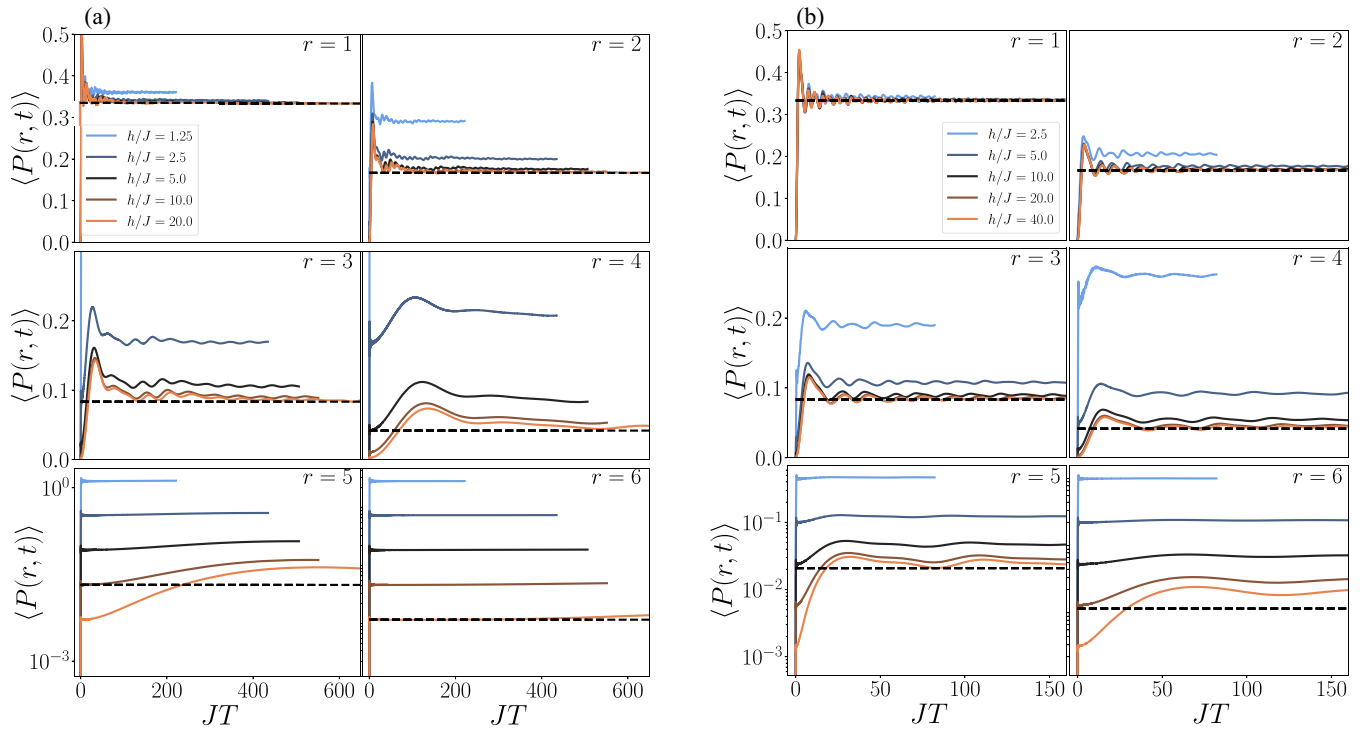
FIG. 4. The average number of particles at hierarchical distance $r$ from the first site, averaged in a time window $t \in [0, T]$. Distinct values of $r$ are shown for a chain of length $L = 64$. The values of $\sigma$ are (a) $\sigma = 2$ and (b) $\sigma = 1$. The TDVP results (solid lines) approach the analytical prediction for large $h/J$ and small $r$. Notice how the scale of the plots is linear for $r \leqslant 4$, while it is logarithmic for $r > 4$, in order to enhance the small values of $\langle P(r, t) \rangle$.

## V. CONCLUSIONS AND OUTLOOKS

In this work, we analyzed a localization phenomenon in a hierarchical long-range model. We were able to construct analytically the single-particle wave function, describing the evolution of a defect in the deep paramagnetic phase, and we provided some bounds, together with the long-time averages, to give a quantitative description of the localization mechanism. Moreover, the universal scaling property in Eq. (18) was found and was traced back to the self-similarity of the hierarchical tree structure.

This work paves the way to further possible investigations. There are still some open questions to be addressed. In particular, from our derivation, it is not clear whether the localization is just a single-particle effect [46]—completely



FIG. 5. As in Fig. 4 for large $JT$. The green line is the theoretical prediction obtained in the single-particle picture. The number of defects increases for a decreasing value of $h$, thus showing deviations from the single-particle picture. (a) $\sigma = 2$ and (b) $\sigma = 1$.

characterized by the eigenfunctions of the hopping matrix—or a true many-body localization (MBL) effect [47–49].

We believe that the symmetry of the hierarchical tree is a key ingredient for these phenomena, and a systematic investigation of its consequences at the level of the many-body spectrum deserves more attention. For instance, it is reasonable that the Hilbert space of this model is fragmented and a huge number of Krylov spaces are present [50]. Moreover, another consequence of the tree symmetry could be the presence of many local integrals of motion, which prevent the thermalization of the system, making the hierarchical model more similar to a disordered system than a translationally invariant long-range one.

Another interesting direction could be the investigation of the dynamics after a global (or local) quench, near the critical point. That would be a way to probe the properties of the system in the middle of the spectrum, not just in the single-particle low-energy band. However, this is a much more difficult protocol for which we do not expect to find exact analytical predictions. One possibility to overcome this problem could be the application of SDRG techniques: however, it is still unclear how to adapt the formalism of [33] besides the ground state to tackle systematically higher-energy states. Another possibility relies on the relation between this model and a $p$-adic field theory [37,38], which could be a way to tackle directly the scaling limit at criticality.

Last, but not least, it could be interesting to study the free-fermionic counterpart of the hierarchical Ising model. We think that beyond the single-particle localization, which should show identical features for both models, some
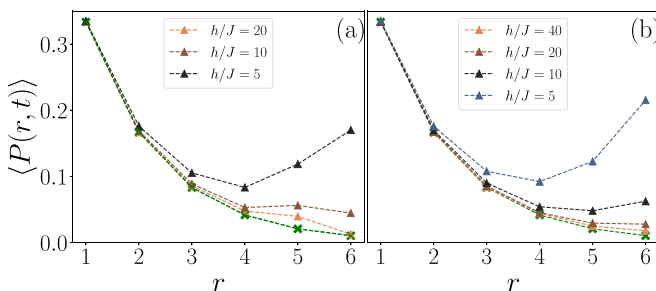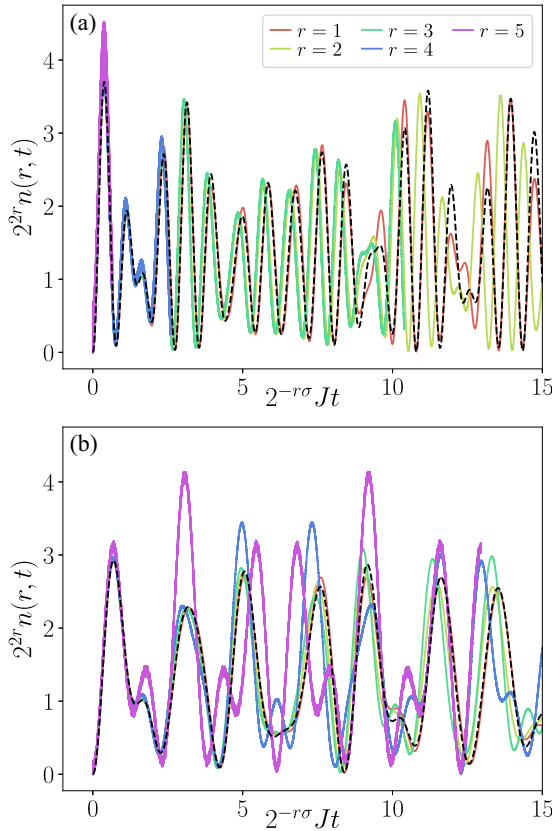
FIG. 6. The behavior of $2^{2r}n(r,t)$, which is expected to be a universal function for large $h/J$, large $N$, and fixed $r$. The dashed line marks the theoretical prediction of the universal function, while the solid lines refer to the numerical data for distinct values of $r$. We consider the parameters (a) $\sigma = 2$, $h = 20J$ and (b) $\sigma = 1$, $h = 40J$. Generally good agreement is found for small $r$, while bigger deviations are found at $r > 4$, probably due mostly to finite-size effects.

many-body properties could also be similar and eventually could be related to the same tree symmetry. The advantage of this approach is the presence of well-established free-fermionic techniques [51] which could shed some light on the quantitative characterization of the conjectured MBL phase of this model. Still, it is not clear which techniques can be successfully applied to make up for the lack of translational symmetry. In conclusion, we believe that a large class of hierarchical quantum models could actually show properties that are similar to those of disordered systems, and a better understanding of their common features may be a huge step toward the solution of some open questions regarding MBL [52].

The data that support the plots within this paper and other findings of this study are available from the authors upon request. The code is available at [53].

## APPENDIX A: DIAGONALIZATION OF THE HOPPING MATRIX

In this Appendix, we analyze the spectrum of the hopping matrix whose matrix elements read

$$
\mathbb{J}_{ij} = \begin{cases} -\dfrac{J}{2^{(1+\sigma)(r(i,j)-1)}} & i \neq j, \\[2mm] 0 & \text{otherwise,} \end{cases} \tag{A1}
$$

for a finite value of the length $L = 2^N$. Here we follow closely Ref. [54], where a similar matrix was considered and the set of eigenvectors and eigenvalues was provided. A remarkable consequence of the hierarchical structure of the hopping is that the set of eigenvectors does not depend explicitly on the values of the interaction terms at distinct levels, and it is completely fixed by symmetry arguments. This mechanism is somehow analogous to translationally invariant systems, in which the single-particle spectrum is diagonalized in Fourier space.

The lowest-energy eigenstate, identified by an index $k = 0$, is given by the wave function

$$
\frac{1}{\sqrt{L}} \chi_{[1,L]}(x), \tag{A2}
$$

which represents single-particle state completely invariant under the symmetries of the tree. Similarly, the wave function

$$
\frac{1}{\sqrt{L}} [\chi_{[1,L/2]}(x) - \chi_{[L/2+1,L]}(x)], \tag{A3}
$$

associated with the index $k = 1$, is an eigenstate which is invariant under the symmetries of the tree which do not mix the left and right half chains, and it is odd under the following permutation of sites:

$$
1 \leftrightarrow L+1, \ldots, \frac{L}{2} \leftrightarrow L. \tag{A4}
$$

Beyond the previous eigenstates, there are multiplets of wave functions that generate degenerates eigenspaces of the hopping matrix. For instance, we can show that the states

$$
\sqrt{\frac{2}{L}} [\chi_{[1,L/4]}(x) - \chi_{[L/2+1,L/2]}(x)],
$$
$$
\sqrt{\frac{2}{L}} [\chi_{[L/2+1,3L/4]}(x) - \chi_{[3L/4+1,L]}(x)], \tag{A5}
$$

associated with $k = 2$, are exactly degenerate. Despite the fact that it is a matter of convention to choose them as a basis of the associated eigenspace, for practical applications it is convenient to do so. Indeed, whenever a single-particle state is localized in the first half chain, its projection over $\chi_{[L/2+1,3L/4]}(x) - \chi_{[3L/4+1,L]}(x)$ vanishes identically, which means that the latter state does not participate explicitly in the dynamical evolution. Similarly, we can show that a multiplet

of the four states ($k = 3$)

$$\sqrt{\frac{4}{L}}[\chi_{[1,L/8]}(x) - \chi_{[L/8+1,L/4]}(x)],$$

$$\sqrt{\frac{4}{L}}[\chi_{[L/4+1,3L/8]}(x) - \chi_{[3L/8+1,L/2]}(x)],$$

$$\sqrt{\frac{4}{L}}[\chi_{[L/2+1,5L/8]}(x) - \chi_{[5L/8+1,3L/4]}(x)], \quad \text{(A6)}$$

$$\sqrt{\frac{4}{L}}[\chi_{[3L/4+1,7L/8]}(x) - \chi_{[7L/8+1,L]}(x)]$$

generates an eigenspace. The discussion can be straightforwardly generalized, showing that for $k \geqslant 1$ the $k$th eigenspace has degeneracy

$$2^{k-1}, \quad k = 1, \ldots, N. \quad \text{(A7)}$$

Given the eigenstates of $-J_{ij}$, the computation of its eigenvalues $\epsilon_k$ in (10) is just a matter of algebra. Indeed, for $k = 0$ we can show that the associated single-particle energy $\epsilon_0$ is just the interaction energy between the first site and the rest of the chain, namely,

$$\epsilon_0 = -\sum_{j=2}^{L} \frac{J}{2^{(1+\sigma)(r(1,j)-1)}}, \quad \text{(A8)}$$

which can be rewritten as a sum over sites at hierarchical distance $r$ as follows:

$$\epsilon_0 = -\sum_{j=2}^{L} 2^{r-1} \frac{J}{2^{(1+\sigma)(r-1)}} = -\frac{J}{1-2^{-\sigma}}(1 - L^{-\sigma}). \quad \text{(A9)}$$

Similarly, for $k = 1$ we have to compute the interaction term between the first site and the other ones belonging to the left chain, adding to this quantity the interactions with the sites of the right half chain with the opposite sign. In other words,

$$\epsilon_1 = -\sum_{j=2}^{L/2} 2^{r-1} \frac{J}{2^{(1+\sigma)(r-1)}} + \frac{L}{2} \frac{J}{2^{(1+\sigma)(N-1)}}$$

$$= -\frac{J}{1-2^{-\sigma}}\left(1 - \frac{2^\sigma}{L^\sigma}\right) + \frac{2^\sigma}{L^\sigma}. \quad \text{(A10)}$$

Similar arguments can be applied for $k \geqslant 2$, and in the end the eigenvalues can be compactly written as

$$\epsilon_k = -\frac{J}{1-2^{-\sigma}}\left(1 - \frac{2^{k\sigma}}{L^\sigma}\right) + J\frac{2^{k\sigma}}{L^\sigma}(1 - \delta_{k,0}) \quad \text{(A11)}$$

for $k = 1, \ldots, N$. From the explicit expression of $\epsilon_k$ we notice that (at least for $\sigma \neq 0$) whenever $k \neq k'$,

$$\epsilon_k \neq \epsilon_{k'}, \quad \text{(A12)}$$

which means that distinct multiplets previously identified are not degenerate among each other. We emphasize that this is not a direct consequence of the tree structure of the hopping matrix, although it can be regarded as a generic property in the absence of a fine tuning of the parameters $J_p$ in (2).

To conclude this Appendix we observe that the decomposition of the delta function
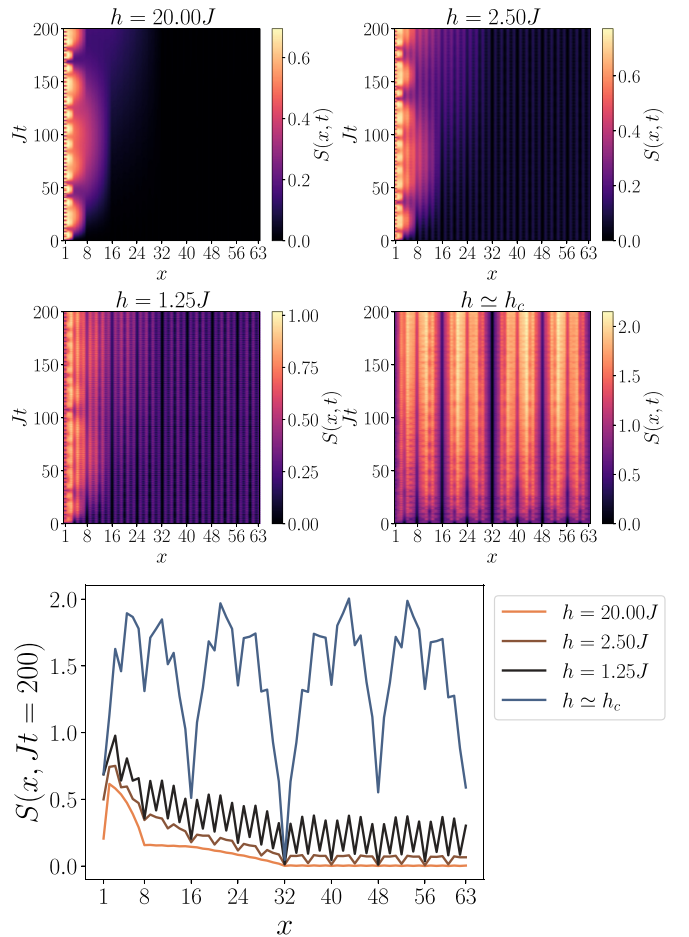
$$\delta_{x,1} \quad \text{(A13)}$$



FIG. 7. Color plots: Entanglement entropy $S(x,t)$ of the bipartition $[1,x] \cup [x+1,L]$ as a function of $x$ and time $t$. Line plot: Entanglement entropy for fixed $Jt = 200$. The value $\sigma = 2$ and different values of $h/J$ are plotted. The localization of the particle is manifest for large $h/J$, while the creation of pairs along the whole chain is enhanced as $h/J$ approaches its critical value.

in terms of the eigenvectors [see (7)] contains exactly one basis element for each multiplet. This is the crucial property at the origin of this single-body localization. Indeed, as $k$ approaches $N$, the eigenstates become more and more localized, and their overlap with the $\delta$ function become nonvanishing in the thermodynamic limit

$$N \to \infty, \quad N - k \text{ fixed.} \quad \text{(A14)}$$

For this reason, the contribution of the localized eigenstates is the relevant one, while the one from the completely delocalized eigenfunctions (say, $k = 0, 1$) is negligible.

## APPENDIX B: ENTANGLEMENT ENTROPY

In this Appendix, we briefly discuss how the mechanism of localization affects the dynamics of the entanglement. To do that, we start from the prediction single-particle wave function in (9), and we express the entanglement entropy in terms of it.

More precisely, let us consider a spatial subsystem $A$ made by a subset of the chain and a state $|\Psi\rangle$. The entanglement

entropy is defined as

$$S(A) = -\text{Tr}(\rho_A \log \rho_A), \tag{B1}$$

with $\rho_A \equiv \text{Tr}_{\bar{A}}(|\Psi\rangle \langle\Psi|)$ being the reduced density matrix of the state $|\Psi\rangle$ and log being the natural logarithm. We now assume that the state $|\Psi\rangle$ is a superposition of states of the form

$$|\uparrow \dots \uparrow\downarrow\uparrow \dots \uparrow\rangle, \tag{B2}$$

describing a single defect at the position $j = 1, \dots, L$ of the chain. It is possible to show that in this case the entanglement entropy is precisely

$$S(A) = -P_A \log P_A - (1 - P_A) \log(1 - P_A), \tag{B3}$$

where $P_A$ is the probability to find the defect inside region $A$. In other words, in terms of the single-particle wave function $\psi(x, t)$ we express $P_A$ as follows:

$$P_A \equiv \sum_{x \in A} |\psi(x, t)|^2. \tag{B4}$$

Taking $A = [1, \dots, x]$ and using the scaling relation (18), we get

$$P_A = \sum_{x'=1}^{x} |\psi(x', t)|^2 \leqslant \sum_{x'=1}^{x} \frac{C}{x'^2} \tag{B5}$$

for a certain constant $C$ which does not depend on the time. This upper bound for the probability $P_A$ goes to zero as $x$ grows, with similar behavior for entanglement entropy. In particular a rough estimation gives the following scaling:

$$1 - P_A \sim \frac{1}{x}, \quad S_A \sim \frac{\log x}{x} \tag{B6}$$

for large values of $x$.

Here we stress explicitly that the conclusion we made is based on the assumption that the one-particle effects are the only relevant ones and that the one-particle wave function shows localization properties at an arbitrary time.

In Fig. 7 we plot the evolution of the entanglement entropy obtained with TDVP for some values of the magnetic field $h$ and $\sigma = 2$. We observe that while for large values of $h$ the entanglement growth at large $x$ is suppressed, for smaller $h$ this is not the case. Indeed, for these values of $h$ entanglement is generated suddenly at arbitrary distances, which is due to pair productions.

[1] A. Campa, T. Dauxois, D. Fanelli, and S. Ruffo, *Physics of Long-Range Interacting Systems* (Oxford University Press, Oxford, 2014).

[2] J. Zhang, P. W. Hess, A. Kyprianidis, P. Becker, A. Lee, J. Smith, G. Pagano, I. D. Potirniche, A. C. Potter, A. Vishwanath, N. Y. Yao, and C. Monroe, Observation of a discrete time crystal, Nature (London) **543**, 217 (2017).

[3] K. Baumann, C. Guerlin, F. Brennecke, and T. Esslinger, Dicke quantum phase transition with a superfluid gas in an optical cavity, Nature (London) **464**, 1301 (2010).

[4] N. Defenu, Metastability and discrete spectrum of long-range systems, Proc. Natl. Acad. Sci. U.S.A. **118**, e2101785118 (2021).

[5] A. Santini, G. Giachetti, and L. Casetti, Violent relaxation in the Hamiltonian mean field model: II. Non-equilibrium phase diagrams, J. Stat. Mech. (2022) 013210.

[6] J. Rovny, R. L. Blum, and S. E. Barrett, Observation of Discrete-Time-Crystal Signatures in an Ordered Dipolar Many-Body System, Phys. Rev. Lett. **120**, 180603 (2018).

[7] S. Choi, J. Choi, R. Landig, G. Kucsko, H. Zhou, J. Isoya, F. Jelezko, S. Onoda, H. Sumiya, V. Khemani, C. von Keyserlingk, N. Y. Yao, E. Demler, and M. D. Lukin, Observation of discrete time-crystalline order in a disordered dipolar many-body system, Nature (London) **543**, 221 (2017).

[8] M. Collura, A. De Luca, D. Rossini, and A. Lerose, Discrete Time-Crystalline Response Stabilized by Domain-Wall Confinement, Phys. Rev. X **12**, 031037 (2022).

[9] G. Giachetti, A. Solfanelli, L. Correale, and N. Defenu, High-order time crystal phases and their fractal nature, arXiv:2203.16562.

[10] G. Giachetti, N. Defenu, S. Ruffo, and A. Trombettoni, Berezinskii-Kosterlitz-Thouless Phase Transitions with Long-Range Couplings, Phys. Rev. Lett. **127**, 156801 (2021).

[11] N. Defenu, A. Trombettoni, and A. Codello, Fixed-point structure and effective fractional dimensionality for O(N) models with long-range interactions, Phys. Rev. E **92**, 052113 (2015).

[12] A. Safavi-Naini, R. J. Lewis-Swan, J. G. Bohnet, M. Gärttner, K. A. Gilmore, J. E. Jordan, J. Cohn, J. K. Freericks, A. M. Rey, and J. J. Bollinger, Verification of a Many-Ion Simulator of the Dicke Model through Slow Quenches across a Phase Transition, Phys. Rev. Lett. **121**, 040503 (2018).

[13] A. Keesling, A. Omran, H. Levine, H. Bernien, H. Pichler, S. Choi, R. Samajdar, S. Schwartz, P. Silvi, S. Sachdev, P. Zoller, M. Endres, M. Greiner, V. Vuletić, and M. D. Lukin, Quantum Kibble-Zurek mechanism and critical dynamics on a programmable Rydberg simulator, Nature (London) **568**, 207 (2019).

[14] J. Schachenmayer, B. P. Lanyon, C. F. Roos, and A. J. Daley, Entanglement Growth in Quench Dynamics with Variable Range Interactions, Phys. Rev. X **3**, 031015 (2013).

[15] S. Pappalardi, A. Russomanno, B. Žunkovič, F. Iemini, A. Silva, and R. Fazio, Scrambling and entanglement spreading in long-range spin chains, Phys. Rev. B **98**, 134303 (2018).

[16] A. Lerose and S. Pappalardi, Origin of the slow growth of entanglement entropy in long-range interacting spin systems, Phys. Rev. Res. **2**, 012041(R) (2020).

[17] G. Giachetti and N. Defenu, Entanglement propagation and dynamics in non-additive quantum systems, arXiv:2112.11488.

[18] S. Scopa, P. Calabrese, and A. Bastianello, Entanglement dynamics in confining spin chains, Phys. Rev. B **105**, 125413 (2022).

[19] C. Monroe, W. C. Campbell, L.-M. Duan, Z.-X. Gong, A. V. Gorshkov, P. W. Hess, R. Islam, K. Kim, N. M. Linke, G. Pagano, P. Richerme, C. Senko, and N. Y. Yao, Programmable quantum simulations of spin systems with trapped ions, Rev. Mod. Phys. **93**, 025001 (2021).

[20] F. Mivehvar, F. Piazza, T. Donner, and H. Ritsch, Cavity QED with quantum gases: New paradigms in many-body physics, Adv. Phys. **70**, 1 (2021).

[21] N. Defenu, T. Donner, T. Macrì, G. Pagano, S. Ruffo, and A. Trombettoni, Long-range interacting quantum systems, arXiv:2109.01063.

[22] D. Lynden-Bell, Statistical mechanics of violent relaxation in stellar systems, Mon. Not. R. Astron. Soc. **136**, 101 (1967).

[23] G. Giachetti, A. Santini, and L. Casetti, Coarse-grained collisionless dynamics with long-range interactions, Phys. Rev. Res. **2**, 023379 (2020).

[24] J. Barré, A. Olivetti, and Y. Y. Yamaguchi, Corrigendum: Algebraic damping in the one-dimensional Vlasov equation, J. Phys. A **45**, 069501 (2012).

[25] L. Onsager, Statistical hydrodynamics, Nuovo Cimento **6**, 279 (1949).

[26] J. W. Britton, B. C. Sawyer, A. C. Keith, C. C. J. Wang, J. K. Freericks, H. Uys, M. J. Biercuk, and J. J. Bollinger, Engineered two-dimensional Ising interactions in a trapped-ion quantum simulator with hundreds of spins, Nature (London) **484**, 489 (2012).

[27] M. A. Baranov, M. Dalmonte, G. Pupillo, and P. Zoller, Condensed matter theory of dipolar quantum gases, Chem. Rev. **112**, 5012 (2012).

[28] R. Landig, L. Hruby, N. Dogra, M. Landini, R. Mottl, T. Donner, and T. Esslinger, Quantum phases from competing short- and long-range interactions in an optical lattice, Nature (London) **532**, 476 (2016).

[29] F. Dyson, Existence of a phase-transition in a one-dimensional Ising ferromagnet, Commun. Math. Phys. **12**, 91 (1969).

[30] D. Kim and C. J. Thompson, Critical properties of Dyson hierarchical model, J. Phys. A **10**, 1579 (1977).

[31] C. Monthus and T. Garel, A critical Dyson hierarchical model for the Anderson localization transition, J. Stat. Mech. (2011) P05005.

[32] F. Iglói and C. Monthus, Strong disorder rg approach–A short review of recent developments, Eur. Phys. J. B **91**, 1 (2018).

[33] C. Monthus, Real-space renormalization for the finite temperature statics and dynamics of the Dyson long-ranged ferromagnetic and spin-glass models, J. Stat. Mech. (2016) 043302.

[34] S. Pappalardi, P. Calabrese, and G. Parisi, Entanglement entropy of the long-range Dyson hierarchical model, J. Stat. Mech. (2019) 073102.

[35] P. G. O. Freund and E. Witten, Adelic string amplitudes, Phys. Lett. B **199**, 191 (1987).

[36] S. S. Gubser, J. Knaute, S. Parikh, A. Samberg, and P. Witaszczyk, p-adic AdS/CFT, Commun. Math. Phys. **352**, 1019 (2017).

[37] M. Heydeman, M. Marcolli, I. Saberi, and B. Stoica, Tensor networks, p-adic fields, and algebraic curves: Arithmetic and the AdS$_3$/CFT$_2$ correspondence, Adv. Theor. Math. Phys. **22**, 93 (2018).

[38] L.-Y. Hung, W. Li, and C. M. Melby-Thompson, p-adic CFT is a holographic tensor network, J. High Energy Phys. 04 (2019) 170.

[39] C. Monthus, Dyson hierarchical long-ranged quantum spin-glass via real-space renormalization, J. Stat. Mech. (2015) P10024.

[40] U. Schollwöck, The density-matrix renormalization group in the age of matrix product states, Ann. Phys. (NY) **326**, 96 (2011).

[41] J. Haegeman, J. I. Cirac, T. J. Osborne, I. Pižorn, H. Verschelde, and F. Verstraete, Time-Dependent Variational Principle for Quantum Lattices, Phys. Rev. Lett. **107**, 070601 (2011).

[42] J. Haegeman, C. Lubich, I. Oseledets, B. Vandereycken, and F. Verstraete, Unifying time evolution and optimization with matrix product states, Phys. Rev. B **94**, 165116 (2016).

[43] S. Paeckel, T. Köhler, A. Swoboda, S. R. Manmana, U. Schollwöck, and C. Hubig, Time-evolution methods for matrix-product states, Ann. Phys. (NY) **411**, 167998 (2019).

[44] F. Fröwis, V. Nebendahl, and W. Dür, Tensor operators: Constructions and applications for long-range interaction systems, Phys. Rev. A **81**, 062337 (2010).

[45] C. Hubig, I. P. McCulloch, and U. Schollwöck, Generic construction of efficient matrix product operators, Phys. Rev. B **95**, 035129 (2017).

[46] P. W. Anderson, Absence of diffusion in certain random lattices, Phys. Rev. **109**, 1492 (1958).

[47] I. V. Gornyi, A. D. Mirlin, and D. G. Polyakov, Interacting Electrons in Disordered Wires: Anderson Localization And Low-$t$ Transport, Phys. Rev. Lett. **95**, 206603 (2005).

[48] D. Basko, I. Aleiner, and B. Altshuler, Metal-insulator transition in a weakly interacting many-electron system with localized single-particle states, Ann. Phys. (NY) **321**, 1126 (2006).

[49] V. Oganesyan and D. A. Huse, Localization of interacting fermions at high temperature, Phys. Rev. B **75**, 155111 (2007).

[50] S. Moudgalya, B. Bernevig, and N. Regnault, Quantum many-body scars and Hilbert space fragmentation: A review of exact results, Rep. Prog. Phys. **85**, 086501 (2022).

[51] V. Eisler and I. Peschel, Evolution of entanglement after a local quench, J. Stat. Mech. (2007) P06005.

[52] D. Abanin, J. Bardarson, G. De Tomasi, S. Gopalakrishnan, V. Khemani, S. Parameswaran, F. Pollmann, A. Potter, M. Serbyn, and R. Vasseur, Distinguishing localization from chaos: Challenges in finite-size systems, Ann. Phys. (NY) **427**, 168415 (2021).

[53] A. Santini, Alessandro-santini/TenNet: Version 0.1.0 (v0.1.0), Zenodo (2022), doi:10.5281/zenodo.6797864.

[54] E. Agliari and F. Tavani, The exact Laplacian spectrum for the Dyson hierarchical network, Sci. Rep. **7**, 39962 (2016).